Dalton Transactions

ROYAL SOCIETY OF CHEMISTRY

PAPER

View Article Online
View Journal | View Issue

Cite this: *Dalton Trans.*, 2021, **50**, 11291

Controlling the molecular diffusion in MOFs with the acidity of monocarboxylate modulators†

Isabel Abánades Lázaro, *‡[a] Catalin Popescu [b] and Francisco G. Cirujano *‡[a]

Received 31st May 2021,
Accepted 14th July 2021

DOI: 10.1039/d1dt01773j

rsc.li/dalton

The catalytic performance of metal–organic frameworks (MOFs) is related to their physicochemical properties, such as particle size, defect chemistry and porosity, which can be potentially controlled by coordination modulation. By combining PXRD, ^{1}HNMR, FT-IR, and N_2 uptake measurements we have gained insights into the control of different types of defects (missing linker or missing cluster consequence of the spatial distribution of missing linkers, and a combination of both) by the type of modulator employed. We show that the molar percent of defects, either as missing linkers or as a part of missing cluster defects, is related to the acidity of a modulator and its subsequent incorporation into the UiO-66 structure. Modulators with strong acidity and small size result in a considerable defect induction that causes an increase in the external surface area and mesopore volume, which is beneficial for the ring-opening of epoxides with amines, using UiO-66 defect-modulated MOFs as heterogeneous catalysts.

Introduction

Coordination modulation of Metal–Organic Frameworks (MOFs)[1] – highly stable, porous hybrid structures composed of metal clusters linked by multidentate organic ligands[2–4] – has emerged as a defect engineering tool to enhance their applications and has received notable attention in the last decade.[5–7] Defects in Zr MOFs were first reported in 2011[8] by thermogravimetric analysis of modulated Zirconium UiO-66 MOFs revealing a linker deficiency, which was further agreed by EXAFS showing a loss of ligands in the first Zr coordination shell, compensated by monotopic ligands, the so-called modulators. Modulators are typically monotopic ligands that are introduced during MOF synthesis and they compete with multitopic linkers for metal nucleation sites.[9] Coordination modulation was first reported in 2008 for Zn MOFs,[10] was then applied to Zr MOFs in 2011,[11] and has boosted the number of reported MOFs ever since.[9]

Modulators can be attached to the metal clusters of the resultant structure as capping (size-control) and/or defect-compensating ligands, providing functionality to the framework.[12–17] In turn, modulators can also act as crystal growth promoters by controlling the acidity of synthesis media without permanent attachment to metal clusters, increasing the particle size and enhancing the crystallinity.[11] The addition of modulators enables fine-tuning of properties such as size,[18] functionality[15,19] and defect chemistry,[6,14] which are themselves related to the changes in the polydispersity of MOFs,[20] mechanical, thermal, and chemical stabilities,[21,22] porosity[14] and the density of open metal sites,[23,24] beneficial for several applications such as heterogeneous catalysis.[24–28]

Zr MOFs are the benchmark materials regarding defect chemistry due to the high stability of the frameworks towards the reduction of the cluster's coordination number.[29–31] Among them, the UiO series of MOFs[32] (UiO stands for University i Oslo) with UiO-66 (Zr-terephthalate), represented in Fig. 1, can reduce its coordination number from 12-connected to 8, resulting in missing cluster consequence of the spatial distribution of missing linkers within the framework.[30,33] To the best of our knowledge, the spatial organisation of missing linkers into point defects (non-extended linker deficient metal sites) or missing clusters is still not fully understood and controlled, with controversial studies being found in the literature.[29] In fact, while missing clusters have been proposed to be the only type of defect,[14,29] HR-TEM has recently shown the co-existence of different types of defects, as represented in Fig. 1: ordered missing linkers from the 12-connected parent ***fcu*** $4[Zr_6(\mu_3\text{-}O)_4(\mu_3\text{-}OH)_4L_6]$ network into a ***bcu*** 8-connected $4[Zr_6(\mu_3\text{-}O)_4(\mu_3\text{-}OH)_4L_4(Mod)_4]$ net in which all the BDC ligands are removed from the parent structure projected along the ⟨001⟩ axis, the 8-connected missing cluster ***reo*** phase $3[Zr_6O_4(OH)_4L_4(Mod)_4]$ in which one

[a]*Instituto de Ciencia Molecular (ICMol), Universitat de València, Catedrático José Beltrán Martínez no 2, 46980 Paterna, Valencia, Spain.*
E-mail: isabel.abanades@uv.es, francisco.c.garcia@uv.es
[b]*CELLS–ALBA Synchrotron, E-08290 Cerdanyola del Valles, Barcelona, Spain*

†Electronic supplementary information (ESI) available: General experimental details and remarks, detailed synthesis conditions, exhaustive characterisation (PXRD, NMR, FT-IR, TGA, SEM, porosity, polydispersity, and water stability) and relationships between the catalytic activity and the properties of materials. See DOI: 10.1039/d1dt01773j

‡These authors contributed equally.

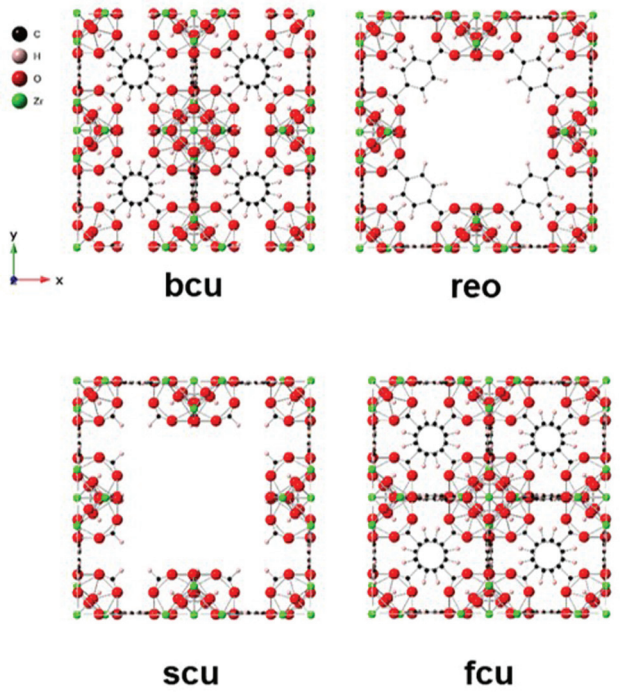

Fig. 1 Ideal UiO-66 phase (fcu) and different defective phases due to missing clusters (reo, scu) or linkers (bcu).

cluster and its connected linkers (L) are missing, with linker being compensated by modulators (Mod), and the 8,4-connected ***scu*** net $3[Zr_6(\mu_3\text{-}O)_4(\mu_3\text{-}OH)_4L_3(Mod)_6]$ of missing cluster defects (Fig. 1).[33] By means of formic acid (FA) modulation, the authors visualized that under their FA modulated conditions the missing linker domains predominate over the missing clusters, with FA defect-compensating modulators attached to the Zr positions. Recent reports have also shown the organization of missing linker defects into other defective phases such as missing cluster defects in the UiO-66 ***hcp*** network with $Zr_{12}(\mu_3\text{-}O)_8(\mu_3\text{-}OH)_8(\mu\text{-}OH)_6$ nodes (paired Zr_6O_8 nodes bridged by the OH groups).[34–36]

Defects play an active role in the chemical reactivity of MOFs, and hence in their catalytic activity.[23,24] Recent reports have shown that defective tetravalent metal sites affect the conversion and selectivity of catalytic processes of industrial relevance, such as the activation of carbonyl groups in the synthesis of biomass-derived platform molecules, biodiesel and other high value-added molecules.[37–39] Point defects at the crystalline positions interrupt the periodicity of the framework, increasing the accessibility to coordinatively unsaturated metal sites that interact with the substrates. The presence of defects is often interconnected with the porosity and particle size (nucleation and crystallisation kinetics),[40] which have a clear incidence on the molecular transport in and out of the active sites. In the particular case of zirconium-based MOFs, the defective metal-oxo clusters have Lewis/Brønsted acidity which can be controlled by the use of modulators (*e.g.* monocarboxylic acids), mineral acids, water, zirconium precursors, temperature, time, *etc*. under synthetic and post-synthetic conditions.[23,24,27,41]

Although the catalytic performance of the defect-containing metal-oxo clusters is related to the bulk physicochemical properties of the materials, studies that enclose both detailed rationalisation of properties based on the synthetic conditions and the interrelationship with the catalytic performance of MOFs are imperative to provide insights into the control of the interrelationship between synthesis, properties and function, which will lead to the design of catalytic MOFs with outstanding performance in relevant catalytic/adsorption solid-based processes. In particular, heterogeneously catalysed synthesis of industrially relevant compounds, such as fine chemicals and pharmaceuticals, through the C–C and C–N bond-forming processes is a recent example where MOFs can bridge state-of-the-art homogeneous catalysts with robust reusable solid catalysts.[39,42,43]

Herein, we study the effects of the acidity and molecular size of modulators on UiO-66 properties in relation to its catalytic performance in the transformation of epoxides into amino alcohols *via* MOF-catalysed C–N bond formation,[36,44–47] aiming to provide insights that will lead to the design of catalytic MOF systems based on their controlled properties. We have chosen UiO-66, a robust system that allows for precise control of its chemical reactivity through defect engineering.[29] The already demonstrated acidic properties of this catalytic platform enable the transformation of many organic compounds through heterogeneous catalytic processes taking place at the nodes of the UiO framework.[24,27,48,49] When a part of the structure is disrupted by the attachment of monocarboxylates, a more open framework is generated, thus favouring the accessibility of active sites in the form of open metal sites (coordinatively unsaturated sites), with sufficient stability due to the high connectivity of the MOF nodes.[14,50]

Results and discussion

In order to induce defects into the UiO-66 structure, we introduced 10 equivalents (with respect to the linker) of well-known defect promoting modulators. We maintained a fixed excess of linker compared to the metal (1.5 equivalents) to reduce the particle size and enhance defect promotion by speeding the metal–linker complexation and subsequent nucleation equilibria.[40] We chose benzoic acid (BA), formic acid (FA) and trifluoroacetic acid (TFA) as modulators, paying special attention to their pK_a values (4.2, 3.7 and 0, respectively) and molecular sizes (see S.2 in the ESI† for detailed synthesis conditions). Note that in the MOF structures FA corresponds to formate, TFA to trifluoroacetate and BA to benzoate. Recent reports have shown that the pK_a values of acetic acid derivatives as modulators are inversely related to the induction of defects in UiO-66,[14] whereas the higher defect promoting activity of benzoic acid than its pK_a analogue, acetic acid, with stoichiometric metal/linker ratios is

attributed to its molecular size, more similar to that of benzene dicarboxylate.[51]

Fig. 2a shows that besides the appearance of sharp Bragg peaks of the UiO-66 framework in the Powder X-Ray Diffraction (PXRD) patterns, the BA and TFA modulated samples showed the existence of a weak broad band (2 theta = 2–3.5), indicated with an arrow. This band, which is considered indicative of the presence of superlattice peaks,[14] is more significant for the TFA modulated sample, whereas it was not apparent upon FA modulation despite having a lower pK_a value than BA (see S.3.1 in the ESI†). The ***reo*** phase has been reported as a broad band at low reflection angles when measured by conventional PXRD, whereas recent reports have shown that both the 8-connected ***reo*** phase and 8,4-connected ***scu*** missing cluster phase simulated PXRD patterns have new reflection bands (100) and (110) at low angles that are absent in both the pristine MOF and the ***bcu*** net of ordered missing linkers.[33] The modulator incorporation into the framework was analysed by combining NMR and FT-IR profiles. NMR (Table 1 and S.3.2 in the ESI†) revealed that the incorporation

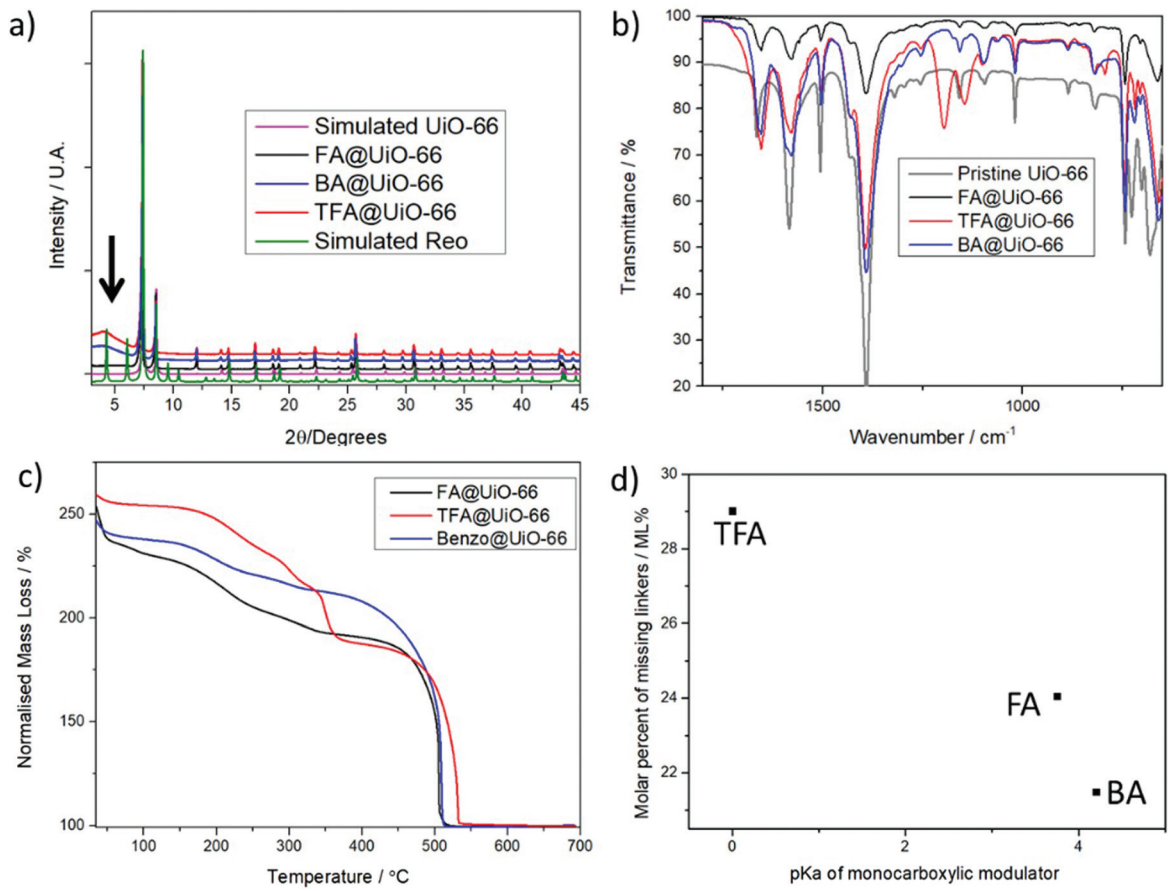

Fig. 2 (a) Stacked PXRD of modulated UiO-66 in comparison with simulated UiO-66 and simulated ***reo*** phase. (b) FT-IR profiles of modulated UiO-66 in comparison with pristine UiO-66. (c) TGA profiles of modulated UiO-66 with metal residue normalized to 100%. (d) Representation of the molar percent of missing linkers in $Zr_6O_4(OH)_4(L)_x(FA)_{XNMR}(Mod)_{XNMR}(OH)_Z(H_2O)_Z$ as a function of the modulator's pK_a, where missing linkers correspond to 6 − *x*, *x* being determined by a combination of NMR analysis of the acid-digested MOF and TGA.

Table 1 Characterisation data extracted by NMR and TGA techniques

Technique	NMR		TGA				
Sample	MOD[a]/L	FA[b]/L	L[c]/Zr_6	MOD/Zr_6	FA/Zr_6	Wt% Zr/DH MOF	ML[d] (%)
BA@UiO-66	0.19	0.22	4.71	0.84	0.91	47.6	21.5
FA@UiO-66	0.29	0.29	4.56	1.33	0.00	52.3	24.1
TFA@UiO-66	0.42*	0.18	4.26	0.92	1.80	54.0	29.0

[a] MOD refers to the modulator. [b] FA refers to formic acid. [c] L refers to linker. [d] ML refers to missing linker. * Since TFA has no protons, a combination of fluor and proton NMR with the presence of a calibrant has been used to calculate the molar ratio between modulator and linker.

of modulators (BA, FA, and TFA) in mole percent (mol%) is inversely related to their pK_a values (Fig. S6 and S7 in the ESI†). However, FA formed by the decomposition of DMF during MOF synthesis is also incorporated into the BA and TFA modulated frameworks, although to a less extent than upon its direct addition, but resulting in a higher number of total monocarboxylate ligands (total modulator) attached to the framework (Fig. S8 in the ESI†). FA co-incorporation compensates for the charge balance upon replacement of ditopic linkers by BA and TFA modulators, possibly making the missing cluster defects more favourable. FT-IR profiles, represented in Fig. 2b (see S.3.3 in the ESI†), show the characteristic vibration bands of the modulators such as the C–F_3 stretching at *ca.* 1195 and 1140 cm^{-1} or the C–F bending at *ca.* 791 cm^{-1}, but the free carboxylate vibration bands are not present due to the modulator attachment to the Zr cluster.

Gravimetric analysis of the thermal decomposition profiles of the MOFs (see S.3.4 in the ESI†), represented in Fig. 2c, revealed a high defectivity in agreement with the high incorporation of monotopic modulators determined by NMR, with the molar percent of missing linkers being directly related to the acidity of the modulators (Fig. 2d) due to their incorporation into the oxo-metallic nodes (see S.3.4 and Fig. S11–18 in the ESI† for detailed explanation of the mathematical models).[52] TGA revealed *ca.* 4.71, 4.56 and 4.26 linkers (6 for the pristine MOF) with the molecular formula $Zr_6O_4(OH)_4(L)_x(FA)_y(Mod)_z(OH)_d(H_2O)_d$ for BA, FA and TFA respectively, corresponding to *ca.* 21, 24 and 29 molar percent of missing linkers (Table 1). In the ***reo*** phase, one cluster and its connected linkers (33.3 molar percent) are removed from the pristine $4[Zr_6(\mu_3\text{-}O)_4(\mu_3\text{-}OH)_4L_6]$ MOF upon replacement by monotopic monocarboxylate modulators (bidentate) or by a combination of bidentate and monodentate monotopic modulators (*i.e.* OH) that coordinate 8 positions in the unit cell with paired neutral species (*i.e.* water, solvent), resulting in 3 $[Zr_6O_4(OH)_4(L)_4(Mod)_4]$ and derivative structures.[14,30]

To rule out the influence of the particle size on the external surface area[53] we measured the particle size of the three modulated MOF samples by Scanning Electron Microscopy (see section S.3.5 in the ESI†) using ImageJ software to analyze the particle size distributions. The average particle size had no statistical significance between sets, as shown in Fig. 3a. This

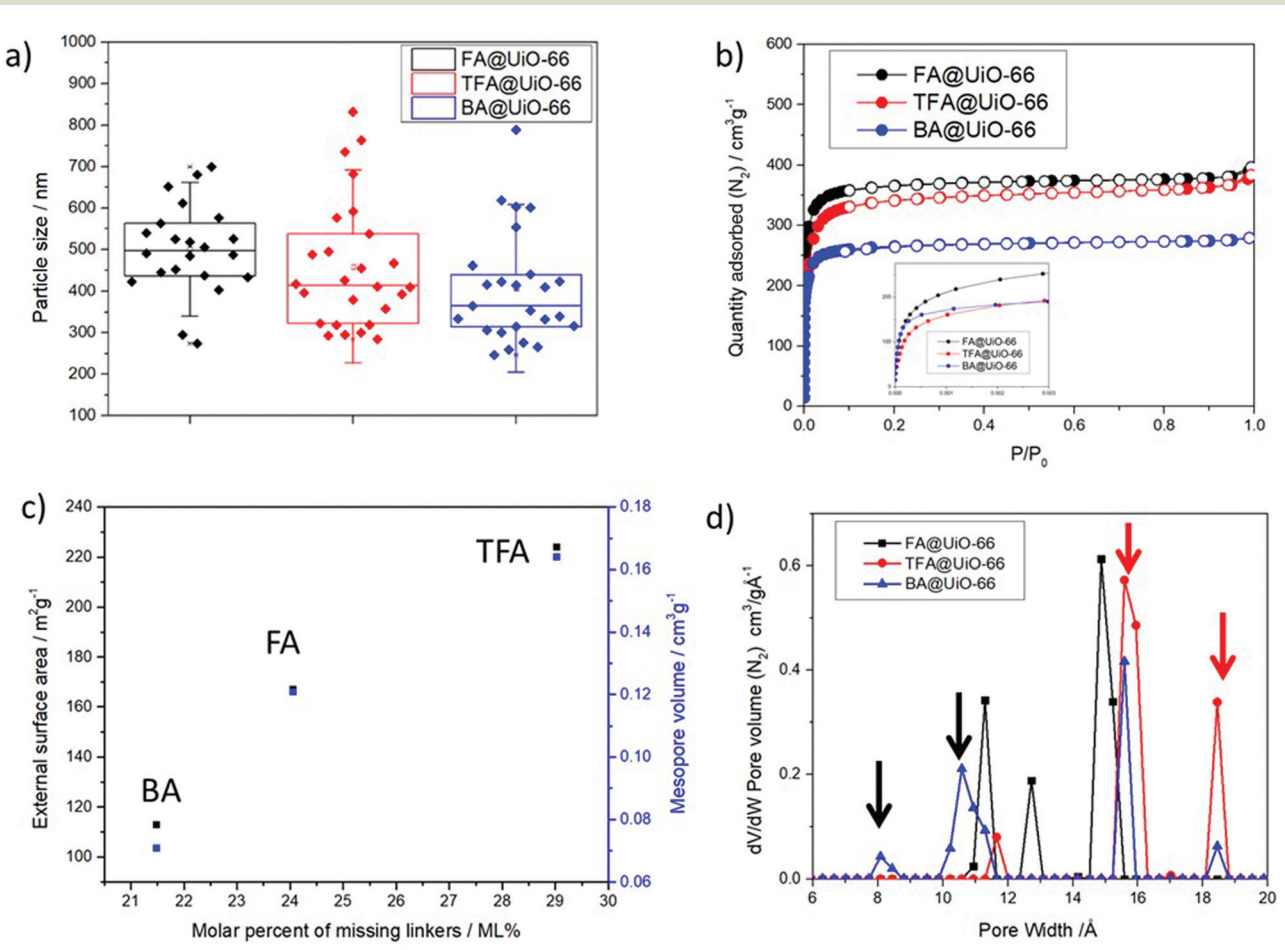

Fig. 3 (a) Statistical box chart of the particle size distributions of modulated UiO-66, showing 25% and 75% quartiles, the average size and the standard distribution. (b) N_2 adsorption and desorption isotherms of modulated UiO-66. (c) Representation of the external surface area and mesopore volume of modulated UiO-66 as a function of the molar percent of missing linkers. (d) Pore size distribution of modulated UiO-66.

indicates that size will not play a role in assessing the differences in their porosities and catalytic activities.[53] Indeed, analysis of the average particle size as a function of incorporation of modulators (Fig. S22 in the ESI†) rules out the influence of the particle size on the external surface area and mesopore volume.

The N_2 adsorption and desorption isotherms (see S.3.6 in the ESI†), represented in Fig. 3b, indicate that the addition of modulators increases the porosity, with S_{BET} of *ca.* 1390 $m^2\ g^{-1}$ upon TFA and FA modulation *vs.* 1200 $m^2\ g^{-1}$ for pristine UiO-66 (Table 2, Fig. S24 in the ESI†). An increase in the porosity rules out the possibility of linker deficiency arising from a metal-rich particle surface. However, the less defective sample (BA) has a smaller S_{BET} value than the pristine MOF. This could be due to the higher volumes and weights of TFA and BA modulators than those of FA[51] and due to the fact that TGA revealed DMF obstruction in the pores of the BA and TFA samples, but not in the pores of the FA sample (see S.3.4 in the ESI† for the assessment of coordinated and obstructed DMF). However, the external surface area and mesopore volume (Table 2) are both proportional to the molar percent of missing linkers, as represented in Fig. 3c, which was previously found to be related to the modulator's acidity, while there was no relationship with the average particle size (Fig. S25 in the ESI†). Although it is known that the external surface area is related to the particle size for small nanoparticles, given that the average particle size of this sample has no statistical difference, together with defects playing an important role in the pore size and opening explains that the external surface area is directly related to the material defect concentration. High external surface areas are beneficial for catalytic applications, where interface phenomena, defective metal sites and intra-crystalline diffusion play major roles, in addition to the micropore area, offering a higher number of accessible active sites at the surface of the nanoparticles.[54,55]

The pore size distributions (PSD) represented in Fig. 3c reveal changes in the pore size distributions from the reported tetrahedral (8 Å) and octahedral (11 Å) pores[32] that indicate nanoregions of missing cluster defects for the TFA and BA modulated samples, which exhibited significant pores at *ca.* 16 and 19 Å, consistent with the reported simulated PSD of the ***reo*** phase.[56] However, while TFA@UiO-66 has completely lost the original pore at 8 Å (and the volume of the 11 Å pore is 3 and 6 times smaller in magnitude than the 16 and 19 Å pores respectively), BA@UiO-66 conserves the pristine MOF pores, which have a similar magnitude to that of the new pores. FA@UiO-66 presents a different PSD, with no tetrahedral 8 Å pore (as TFA) but with new pores at *ca.* 13 and 15 Å, the latter being the most significant of all. Although its bigger pore is similar to the simulated ***reo*** phase (*ca.* 16 Å),[56] its smaller size together with the absence of the ***reo*** 19 Å pore indicates, in great agreement with the absence of a broad band at low angles in the PXRD pattern, that missing clusters are not the most prevalent defects in FA@UiO-66. In addition, the simulated accessible surface area (1360/1612 $m^2\ g^{-1}$) and pore volume (0.503/0.557 $cm^3\ g^{-1}$) for UiO-66 with 9 linkers out of 12 (4.5 out of 6) compensated by FA or OH^- respectively are similar to the experimental porosimetry values of FA@UiO-66 (Table 2), with 9 out of 12 linkers calculated by a combination of TGA and NMR, with missing linkers compensated by a combination of FA and OH^-.[57]

Although TGA provides very good calculations of the molecular formula of the materials, it cannot differentiate between the types of defects (missing linkers and/or missing clusters and their topologies).[29] Based on the previously discussed PXRD, TGA and PSD data, we postulate that BA and TFA induce missing cluster defects upon incorporation, with a partial compensation by FA, while the missing cluster contribution for FA modulation is less significant. The MOF exhibits *ca.* 29% of missing linkers upon modulation with highly acidic TFA, close to 33% of missing linkers for the pure **reo** phase, and its PSD matches well with **reo** simulations, suggesting exclusively missing cluster defects. BA@UiO-66 presents 21% of missing linkers, leading to a smaller degree of missing clusters. However, the preservation of its micropore structure suggests pairing missing linkers that are not part of missing cluster defects. In contrast, when only FA is added in the absence of other modulators, it is incorporated into the MOF structure compensating for missing linker defects, and its spatial distribution does not favour the formation of missing cluster defects under the studied conditions (excess of linker), at least not in a significant manner in the form of nanoregions, as indicated by PXRD and PSD. The differences in the types of defects induced are not related to the pK_a values of the modulators, but could be a consequence of their molecular sizes: steric hindrance due to bigger molecular size favours the attachment of FA (from the decomposition of DMF) and OH/H_2O pairs in close proximity instead of linkers. Although this study encloses 3 modulators, further studies on the relationship between the modulator's molecular size *vs.* pK_a, and the formation of different defective phases in UiO-type MOFs are underway.

Overall, characterisation reveals that while the particle size can be maintained by fixing an excess of linker, the molar percent of defects, their types and distribution could be tuned by the modulator choice. The molar percent of defects and the external surface area are related to the acidity of the modulator and its subsequent incorporation, but its molecular size seems to play a more important role in determining its spatial distri-

Table 2 Characterisation data extracted from the N_2 adsorption/desorption isotherms

Sample	$S_{BET}/S_{MICRO}/S_{EXT}$ ($m^2\ g^{-1}$)	V_{micro}/V_{meso} [a] ($cm^3\ g^{-1}$)		V_t [a] ($cm^3\ g^{-1}$)
BA@UiO-66	1042/929/113	0.362	0.071	0.433
FA@UiO/66	1393/1226/167	0.494	0.121	0.615
TFA@UiO-66	1389/1165/224	0.431	0.164	0.595

[a] V_{micro} was calculated using the *t*-plot model with the Harkins and Jura thickness curve based on the BET surface areas. V_{total} was calculated at $P/P_0 = 0.9$ and $V_{meso} = V_{total} - V_{micro}$.

bution, resulting in missing linker defects for FA and the co-existence of missing linkers and missing clusters for TFA and BA, with its consequent impact on the pore size distribution.

At this point, we investigated the impact of the defect-modulated MOF properties (Zr sites associated with defectivity and related porosity features) on the activation of oxygen and nitrogen-containing substrates (*e.g.* epoxides, alcohols and amines).[58] The resulting Zr open metal sites due to the presence of different modulators allow the transformation of amines and epoxides into pharmaceutically relevant functional molecules like amino alcohols (*i.e.* adrenaline). Hence, we studied the interrelationship between the properties of defective materials and their catalytic performances in the straightforward synthesis of β-amino alcohols through regioselective ring-opening of oxiranes (epoxides) with amines, as represented in Fig. 4a, by reacting cyclohexene oxide with aniline, which was performed at room temperature in EtOH with and without MOF for 24 hours (see S.4 in the ESI† for detailed conditions).

While the non-catalysed reaction between aniline and cyclohexene oxide at room temperature attains a 3% conversion after 24 hours, the defective MOFs are active catalysts for the desired C–N bond formation, reaching a *ca.* 80% conversion for TFA-modulated UiO-66 after 24 hours and *ca.* 59% after 8 hours, as represented in Fig. 4b and c, and tabulated in Table S6 in the ESI.†

Conversion and selectivity are related to MOF defectivity, among other inter-related properties. Fig. 4b and c show that the pK_a value of the modulator is inversely proportional to conversion and directly proportional to selectivity towards the addition of aniline (instead of the alcohol solvent, which may act as a nucleophile in the presence of more defective MOFs). As previously discussed, the pK_a value of the modulator is related to its incorporation and the resultant framework's defectivity – a lower pK_a value results in a higher amount of deprotonated species that are more effective in capping the Zr_6-oxoclusters – and so, the more defective the MOF, the higher the catalytic conversion (Fig. 5a). Replacing linkers by modulators results in the opening of the framework, leading to higher mesopore volumes and external surface areas. This results in more accessible Zr active sites, which are available for the activation of the reaction substrates. Moreover, bulkier modulator molecules, like benzoic acid, occupy more space in the MOF cavities, which results in a significant decrease in the porosity in comparison with light monocarboxylates, *i.e.* formic or trifluoroacetic acid. Thus, the influence of missing linkers on the textural properties of the crystals (improving the diffusion of reactants during the ring-opening of cyclohexene epoxide) is the cause of its improved catalytic performance, as illustrated in Fig. 5b and c. Thus, acidity, defectivity, mesopore volume and external surface area being inter-related properties, all are proportional to the modulated UiO-66 catalytic activity in the order TFA > FA > BA, as illustrated in Fig. 5 and Fig. S28–S31 in the ESI.† The PXRD patterns of the spent materials are similar to those of the as-prepared MOFs, indicating no damage to the structure (Fig. S33 in the ESI†). Additionally, Fig. S34† shows that the high performance TFA@UiO-66 maintains its catalytic activity and selectivity for 4 reaction cycles.

The increase in conversion is notable if we consider previous literature reports showing a 40% conversion in the ring-opening of epoxides after 24 hours at 55 °C for UiO-66 with 1.75 missing linkers out of 12,[58] whereas our conditions are room temperature and reach up to 80% conversion with *ca.* 4 out of 12 missing linkers. To put our results in context, we calculated the TONs per Zr site associated with the defects in the coordination-modulated MOFs reported here. Assuming *ca.*

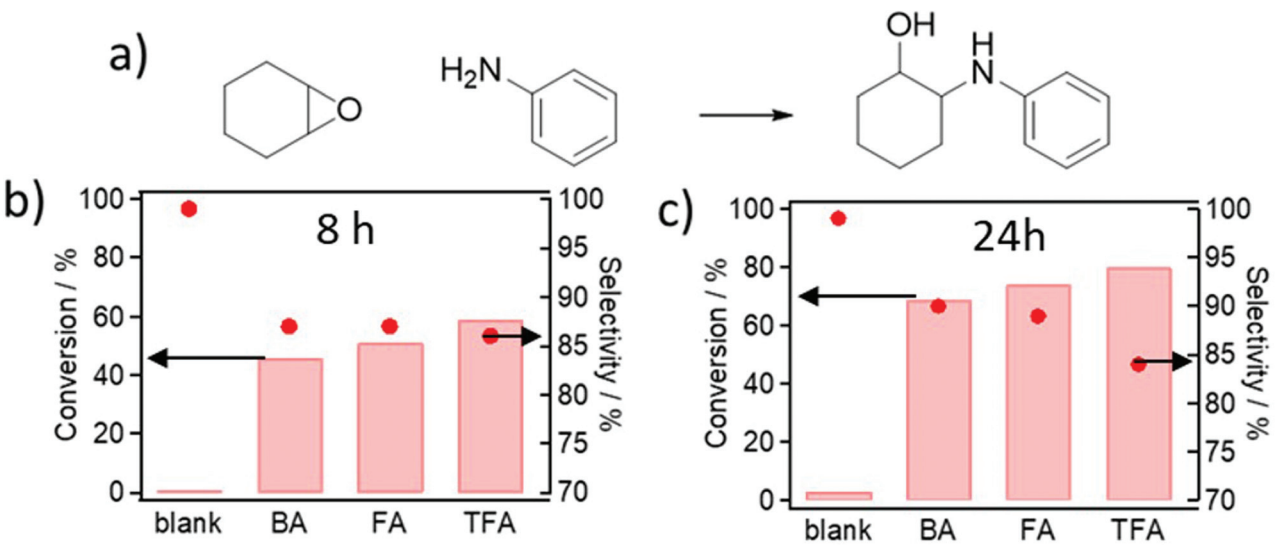

Fig. 4 (a) Conversion of cyclohexene oxide (left axis, red bars) and selectivity to the resulting amino alcohol (right axis, red circles) in the presence of (Zr)UiO-66 catalysts after 8 h (b) or 24 h (c) prepared with three different monocarboxylate modulators (BA = benzoic acid, FA = formic acid, TFA = trifluoroacetic acid).

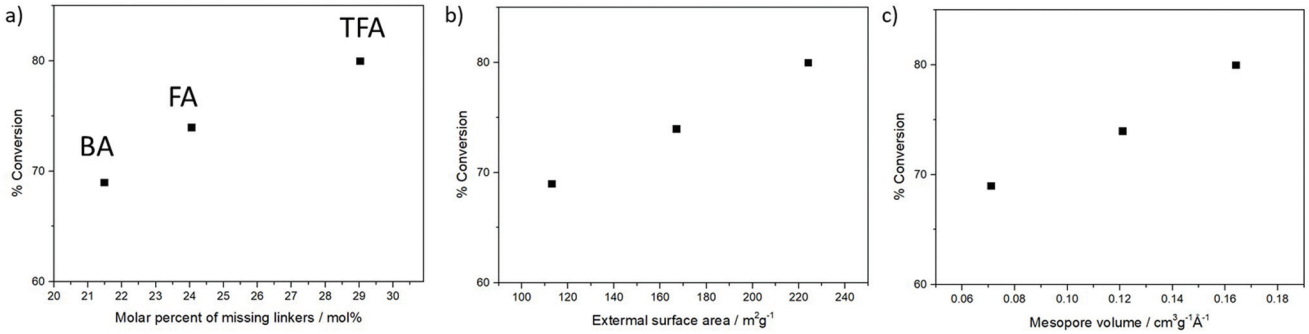

Fig. 5 Relationship between cyclohexene oxide conversion percent after 24 hours and the structural and textural properties of the UiO type MOFs: molar percent of missing linkers (a), external surface area (b), and mesopore volume (c).

30 wt% of Zr associated with defective clusters, the TON of these sites is 8, which could be competitive with TONs of 2–20 obtained with the benchmark Zr-MOFs reported in the literature for the same reaction studied here.[44,59]

Conclusions

We have shown the versatility of the MOF-modulated approach in tailoring the porosity of the final material. The pK_a value of monocarboxylate molecules (*e.g.* benzoic, formic and trifluoroacetic acids) used as modulators of crystal growth of zirconium carboxylate frameworks is key to controlling the degree of defects in the crystal. The concentration of defects in the form of missing terephthalate linkers that have been exchanged by the monocarboxylate is inversely proportional to the pK_a value of the modulator. Through defect engineering of the framework, the mesoporosity and external surface area can be tailored to expose a higher number of Zr acid sites readily available to interact with the reactants involved in catalytic processes. Both cyclohexene oxide and aniline diffusion are favoured for the TFA-modulated MOF, which shows improved textural (higher porosity) and, thus, catalytic properties (higher conversion in the ring-opening of epoxides).

Although this study encloses 3 modulators, we encourage MOF researchers to closely look at the relationship between the modulator's molecular size and pK_a, with the formation of different defective phases in UiO-type MOFs. This investigation also suggests that the formation of either missing clusters or missing linkers and their distribution do not drastically affect the catalytic properties of materials, with overall replacement of linkers (in either of the defective phases) and its relationship with the material's porosity driving its catalytic performance.

Author contributions

The manuscript was written through the contributions of all authors. All authors have approved the final version of the manuscript.

Conflicts of interest

There are no conflicts to declare.

Acknowledgements

FGC and IAL thank the University of Valencia, the Instituto de Ciencia Molecular and the FuniMat Research group for research facilities.

FGC acknowledges the project that gave rise to these results and received the support of a fellowship from" La Caixa" Foundation (ID 100010434). The fellowship code is LCF/BQ/PI19/11690011. This project has also received funding from the European Union's Horizon 2020 research and innovation programme under the Marie Skłodowska-Curie grant agreement No 837804. IAL thanks Marie-Curie Actions for the Individual Fellowship 837804 (DefTiMOFs, MSCA-IF-2018).

C. P. is thankful for the financial support from the Spanish MINECO Project No. FIS2017-83295-P. Synchrotron powder X-ray diffraction experiments were performed at the Materials Science and Powder Diffraction beamline of ALBA Synchrotron (Alba Experiment No. 2020094558).[60]

Notes and references

1 S. Dissegna, K. Epp, W. R. Heinz, G. Kieslich and R. A. Fischer, *Adv. Mater.*, 2018, **10**, 1704501–1704524.
2 A. Carné-Sánchez, I. Imaz, K. C. Stylianou and D. Maspoch, *Chem. – Eur. J.*, 2014, **20**, 5192–5201.
3 P. Z. Moghadam, A. Li, X.-W. Liu, R. Bueno-Perez, S. Wang, S. Wiggin, P. A. Wood and D. Fairen-Jimenez, *Chem. Sci.*, 2020, **11**, 8373–8387.
4 S. Wang, C. M. McGuirk, A. d'Aquino, J. A. Mason and C. A. Mirkin, *Adv. Mater.*, 2018, **30**, 2618–2625.
5 Z. Fang, B. Bueken, D. E. D. Vos and R. A. Fischer, *Angew. Chem., Int. Ed.*, 2015, **54**, 7234–7254.
6 G. Cai and H.-L. Jiang, *Angew. Chem., Int. Ed.*, 2017, **56**, 563–567.

7 W. Xiang, Y. Zhang, Y. Chen, C. Liu and X. Tu, *J. Mater. Chem. A*, 2020, **8**, 21526–21546.
8 L. Valenzano, B. Civalleri, S. Chavan, S. Bordiga, M. H. Nilsen, S. Jakobsen, K. P. Lillerud and C. Lamberti, *Chem. Mater.*, 2011, **23**, 1700–1718.
9 R. S. Forgan, *Chem. Sci.*, 2020, **11**, 4546–4562.
10 S. Hermes, T. Witte, T. Hikov, D. Zacher, S. Bahnmüller, G. Langstein, K. Huber and R. A. Fischer, *J. Am. Chem. Soc.*, 2007, **129**, 5324–5325.
11 A. Schaate, P. Roy, A. Godt, J. Lippke, F. Waltz, M. Wiebcke and P. Behrens, *Chem. – Eur. J.*, 2011, **17**, 6643–6651.
12 I. A. Lázaro, C. J. R. Wells and R. S. Forgan, *Angew. Chem., Int. Ed.*, 2020, **59**, 5211–5217.
13 I. A. Lázaro, S. Haddad, J. M. Rodrigo-Muñoz, R. J. Marshall, B. Sastre, V. del Pozo, D. Fairen-Jimenez and R. S. Forgan, *ACS Appl. Mater. Interfaces*, 2018, **10**, 31146–31157.
14 G. C. Shearer, S. Chavan, S. Bordiga, S. Svelle, U. Olsbye and K. P. Lillerud, *Chem. Mater.*, 2016, **28**, 3749–3761.
15 M. Taddei, G. M. Schukraft, M. E. A. Warwick, D. Tiana, M. J. McPherson, D. R. Jones and C. Petit, *J. Mater. Chem. A*, 2019, **7**, 23781–23786.
16 I. A. Lázaro, S. Haddad, J. M. Rodrigo-Muñoz, C. Orellana-Tavra, V. del Pozo, D. Fairen-Jimenez and R. S. Forgan, *ACS Appl. Mater. Interfaces*, 2018, **10**, 5255–5268.
17 I. A. Lázaro, N. Almora-Barrios, S. Tatay and C. Martí-Gastaldo, *Chem. Sci.*, 2020, **12**, 2586–2593.
18 C. R. Marshall, S. A. Staudhammer and C. K. Brozek, *Chem. Sci.*, 2019, **10**, 9396–9408.
19 I. A. Lázaro, S. Haddad, S. Sacca, C. Orellana-Tavra, D. Fairen-Jimenez and R. S. Forgan, *Chem*, 2017, **2**, 561–578.
20 W. Morris, S. Wang, D. Cho, E. Auyeung, P. Li, O. K. Farha and C. A. Mirkin, *ACS Appl. Mater. Interfaces*, 2017, **9**, 33413–33418.
21 S. Dissegna, P. Vervoorts, C. L. Hobday, T. Düren, D. Daisenberger, A. J. Smith, R. A. Fischer and G. Kieslich, *J. Am. Chem. Soc.*, 2018, **140**, 11581–11584.
22 B. V. de Voorde, I. Stassen, B. Bueken, F. Vermoortele, D. D. Vos, R. Ameloot, J.-C. Tan and T. D. Bennett, *J. Mater. Chem. A*, 2014, **3**, 1737–1742.
23 F. Vermoortele, B. Bueken, G. L. Bars, B. V. de Voorde, M. Vandichel, K. Houthoofd, A. Vimont, M. Daturi, M. Waroquier, V. V. Speybroeck, C. Kirschhock and D. E. D. Vos, *J. Am. Chem. Soc.*, 2013, **135**, 11465–11468.
24 F. G. Cirujano and F. X. L. i Xamena, *J. Phys. Chem. Lett.*, 2020, **11**, 4879–4890.
25 K. Fan, W.-X. Nie, L.-P. Wang, C.-H. Liao, S.-S. Bao and L.-M. Zheng, *Chem. – Eur. J.*, 2017, **23**, 6615–6624.
26 W. Liang, L. Li, J. Hou, N. D. Shepherd, T. D. Bennett, D. D'Alessandro and V. Chen, *Chem. Sci.*, 2018, **9**, 3508–3516.
27 N. Martin and F. G. Cirujano, *Org. Biomol. Chem.*, 2020, **18**, 8058–8073.
28 F. G. Cirujano, M. Stalpaert and D. E. D. Vos, *Green Chem.*, 2018, **20**, 2481–2485.
29 M. Taddei, *Coord. Chem. Rev.*, 2017, **343**, 1–24.
30 M. J. Cliffe, W. Wan, X. Zou, P. A. Chater, A. K. Kleppe, M. G. Tucker, H. Wilhelm, N. P. Funnell, F.-X. Coudert and A. L. Goodwin, *Nat. Commun.*, 2014, **5**, 4176–4184.
31 A. K. Cheetham, T. D. Bennett, F.-X. Coudert and A. L. Goodwin, *Dalton Trans.*, 2016, **45**, 4113–4126.
32 J. H. Cavka, S. Jakobsen, U. Olsbye, N. Guillou, C. Lamberti, S. Bordiga and K. P. Lillerud, *J. Am. Chem. Soc.*, 2008, **130**, 13850–13851.
33 L. Liu, Z. Chen, J. Wang, D. Zhang, Y. Zhu, S. Ling, K.-W. Huang, Y. Belmabkhout, K. Adil, Y. Zhang, B. Slater, M. Eddaoudi and Y. Han, *Nat. Chem.*, 2019, **11**, 622–628.
34 F. C. N. Firth, M. J. Cliffe, D. Vulpe, M. Aragones-Anglada, P. Z. Moghadam, D. Fairen-Jimenez, B. Slater and C. P. Grey, *J. Mater. Chem. A*, 2019, **7**, 7459–7469.
35 M. J. Cliffe, E. Castillo-Martínez, Y. Wu, J. Lee, A. C. Forse, F. C. N. Firth, P. Z. Moghadam, D. Fairen-Jimenez, M. W. Gaultois, J. A. Hill, O. V. Magdysyuk, B. Slater, A. L. Goodwin and C. P. Grey, *J. Am. Chem. Soc.*, 2017, **139**, 5397–5404.
36 X. Chen, Y. Lyu, Z. Wang, X. Qiao, B. C. Gates and D. Yang, *ACS Catal.*, 2020, **10**, 2906–2914.
37 F. G. Cirujano, *Catal. Sci. Technol.*, 2017, **7**, 5482–5494.
38 G. Fu, F. G. Cirujano, A. Krajnc, G. Mali, M. Henrion, S. Smolders and D. De Vos, *Catal. Sci. Technol.*, 2020, **10**, 4002–4009.
39 F. G. Cirujano and N. Martín, *Advanced Functional Solid Catalysts for Biomass Valorization*, Elsevier, Amsterdam, 2020, pp. 187–198.
40 S. Griffin, M. Briuglia, J. ter Horst and R. S. Forgan, *Chem. – Eur. J.*, 2020, **26**, 6910–6918.
41 C. Jia, F. G. Cirujano, B. Bueken, B. Claes, D. Jonckheere, K. M. V. Geem and D. D. Vos, *ChemSusChem*, 2019, **12**, 1256–1266.
42 F. G. Cirujano, R. Luque and A. Dhakshinamoorthy, *Molecules*, 2021, **26**, 1445–1461.
43 F. G. Cirujano, *ChemCatChem*, 2019, **11**, 5671–5685.
44 A. Das, N. Anbu, H. Reinsch, A. Dhakshinamoorthy and S. Biswas, *Inorg. Chem.*, 2019, **58**, 16581–16591.
45 A. Das, N. Anbu, M. Sk, A. Dhakshinamoorthy and S. Biswas, *ChemCatChem*, 2020, **12**, 1789–1798.
46 N. E. Thornburg, Y. Liu, P. Li, J. T. Hupp, O. K. Farha and J. M. Notestein, *Catal. Sci. Technol.*, 2016, **6**, 6480–6484.
47 C. Vignatti, J. Luis-Barrera, V. Guillerm, I. Imaz, R. Mas-Ballesté, J. Alemán and D. Maspoch, *ChemCatChem*, 2018, **10**, 3995–3998.
48 J. N. Hall and P. Bollini, *React. Chem. Eng.*, 2018, **4**, 207–222.
49 F. Vermoortele, R. Ameloot, L. Alaerts, R. Matthessen, B. Carlier, E. V. R. Fernandez, J. Gascon, F. Kapteijn and D. E. D. Vos, *J. Mater. Chem.*, 2012, **22**, 10313–10321.
50 F. G. Cirujano, N. Martin and L. H. Wee, *Chem. Mater.*, 2020, **32**, 10268–10295.
51 C. Atzori, G. C. Shearer, L. Maschio, B. Civalleri, F. Bonino, C. Lamberti, S. Svelle, K. P. Lillerud and S. Bordiga, *J. Phys. Chem. C*, 2017, **121**, 9312–9324.
52 I. A. Lázaro, *Eur. J. Inorg. Chem.*, 2020, **2020**, 4284–4294.

53 M. Taddei, K. C. Dümbgen, J. A. van Bokhoven and M. Ranocchiari, *Chem. Commun.*, 2016, **52**, 6411–6414.
54 N. Martín, M. Dusselier, D. E. D. Vos and F. G. Cirujano, *ACS Catal.*, 2018, **9**, 44–48.
55 Q.-L. Zhu and Q. Xu, *Chem*, 2016, **1**, 220–245.
56 W. Liang, C. J. Coghlan, F. Ragon, M. Rubio-Martinez, D. M. D'Alessandro and R. Babarao, *Dalton Trans.*, 2016, **45**, 4496–4500.
57 A. W. Thornton, R. Babarao, A. Jain, F. Trousselet and F.-X. Coudert, *Dalton Trans.*, 2015, **45**, 4352–4359.
58 Y. Liu, R. C. Klet, J. T. Hupp and O. Farha, *Chem. Commun.*, 2016, **52**, 7806–7809.
59 P. Ji, X. Feng, P. Oliveres, Z. Li, A. Murakami, C. Wang and W. Lin, *J. Am. Chem. Soc.*, 2019, **141**, 14878–14888.
60 F. Fauth, I. Peral, C. Popescu and M. Knapp, *Powder Diffr.*, 2013, **28**, 360–370.